

Bearing capacity of an eccentric tubular concrete-filled steel bridge pier

Weining Sui^{1a}, Haobo Cheng^{2b} and Zhanfei Wang^{*2}

¹ School of civil engineering, Shenyang Jianzhu University, No. 9, Hunnan East Road, Hunnan New District, Shenyang, 110168, China

² Traffic Engineering College, Shenyang Jianzhu University, No. 9, Hunnan East Road, Hunnan New District, Shenyang, 110168, China

(Received July 6, 2017, Revised January 11, 2018, Accepted March 4, 2018)

Abstract. In this paper, the bearing capacity of a non-eccentric and eccentric tubular, concrete-filled, steel bridge pier was studied through the finite element method. Firstly, to verify the validity of the numerical analysis, the finite element analysis of four steel tube columns with concrete in-fill was carried out under eccentric loading and horizontal cyclic loading. The analytical results were compared with experimental data. Secondly, the effects of the eccentricity of the vertical loading on the seismic performance of these eccentrically loaded steel tubular bridge piers were considered. According to the simulated results, with increasing eccentricity ratio, the bearing capacity on the eccentric side of a steel tubular bridge pier (with concrete in-fill) is greatly reduced, while the capacity on the opposite side is improved. Moreover, an empirical formula was proposed to describe the bearing capacity of such bridge piers under non-eccentric and eccentric load. This will provide theoretical evidence for the seismic design of the eccentrically loaded steel tubular bridge piers with concrete in-fill.

Keywords: steel tubular bridge pier; concrete in-fill; bearing capacity; eccentricity; numerical analysis

1. Introduction

Modern urban transportation systems have developed rapidly in China. The steel bridge pier, which has excellent hysteretic behavior, has been widely used in viaducts and beltways. The flexibility of steel bridge pier designs can satisfy the requirement of road programming in modern cities, a number of eccentrically loaded steel bridge pier columns have appeared in viaducts (Fig. 1). Eccentrically loaded steel bridge pier columns would be subjected to pressure, bending, shear and torsion under combined action of the vertical eccentric load from the upper structure and earthquake action, and this affects their seismic performance (Gao *et al.* 2000a). A number of researchers (Gao *et al.* 2000b, Sakimoto *et al.* 2002, Ge *et al.* 2003, Aoki *et al.* 2003, Mamaghani *et al.* 2008) have experimentally and theoretically investigated the seismic capacity of eccentrically loaded steel bridge piers. Their work indicates that the bearing capacity of eccentrically loaded steel bridge pier columns on the eccentric side is greatly decreased, while that on the opposite side is increased. It shows obvious asymmetry, the seismic performance decreases. The ultimate strength and the ductility of the eccentrically loaded steel pipe columns were determined through the transverse load-transverse displacement hysteretic relationship between the centrally and the eccentrically loaded columns (Gao *et al.* 2000a).

On the other hand, a steel bridge pier with concrete in-fill has been proposed to improve the seismic performance of centrally loaded steel bridge piers (Iura *et al.* 2002, Susantha *et al.* 2002, Michel and Julia 2004, Moon *et al.* 2012, Perea *et al.* 2014, Goto *et al.* 2010, 2012, 2014, Wei *et al.* 2014, Wang *et al.* 2011, Nie *et al.* 2012, Shimaguchi and Suzuki 2015, Kim *et al.* 2016) after the 1995 Kobe earthquake. The seismic performance of steel tubular bridge piers with partial concrete filling is better than that of the hollow steel bridge piers (Iura *et al.* 2002). Empirical formulae for the bearing capacity and ductility of centrally loaded steel bridge piers, considered concrete-filling ratio, slenderness ratio, and radius-thickness ratio through eight tests and 60 FEM results, were presented (Wang *et al.* 2015, 2016). If the correlation between centrally and eccentrically loaded pier behaviors can be found, the bearing capacity and ductility of eccentrically loaded columns with partial concrete filling will be conveniently obtained from those of centrally loaded columns. To the writers' knowledge, however, the research on the strength and ductility of eccentrically loaded steel tubular bridge pier with partial concrete filling under cyclic loading remains limited.

The objective of this paper is to find a relationship between the bearing capacities of centrally, and eccentrically, loaded columns and to evaluate the strength and ductility of eccentrically loaded columns by a numerical analytical method. At first, to verify the validity of the numerical analysis, the finite element analyses of four steel tube columns with partial concrete filling was conducted under eccentric loading and horizontal cyclic loading. The analytical results were compared with experimental data. Secondly, a large number of analytical models of the steel tubular bridge piers with partial concrete filling were established to study the effects of the eccentricity. Finally, based on the simulated results,

*Corresponding author, Professor, Dr., Eng.,
E-mail: swnwzf19790627@hotmail.com

^a Associate professor, Dr., Eng.,
E-mail: wzf9522@hotmail.com

^b Master Student, E-mail: 1936634710@qq.com



Fig. 1 An eccentrically loaded steel tubular bridge pier

a formula was proposed with which to describe the bearing capacity relationship between centrally, and eccentrically, loaded steel tubular bridge piers with partial concrete filling.

2. Summary of finite element analysis used

2.1 Analytical models

An inverted L-shaped steel bridge pier (Fig. 1) was taken as the research object, and the analytical model was established in the finite element analysis ABAQUS software package. The finite element model is shown in Fig. 2, where, P is the vertical eccentric loading, H represents the cyclic horizontal loading, h is the column height, l is the eccentricity of the load, and H_0 represents the concrete filling height.

In the analytical model, considering both the computation time and the accuracy of the finite element model, the upper part of the steel tubular bridge pier was simplified as a type-B31 beam element. Some 24 beam elements were used (four for the cantilever beam and 20 for the upper part of the steel tube). The lower part of the steel tubular part, where large local buckling deformations may occur, was simulated by the very small square S4R-type of shell element. The mesh used to model the tube, along the perimeter direction, was divided into 36 elements, and along the longitudinal direction it was refined that the refined concrete-filled segment and hollow segment height is only two thirds of the diameter of the steel tube with a refined element aspect ratio of 3:1. And the in-filled concrete is simulated by C3D8R solid elements, the mesh used to model the concrete, along the radius, was divided into six elements, from the inside out, along the longitudinal direction it was divided in the same way as the steel tube mesh.

A rigid body was used to connect the upper simplified beam element and the lower shell element. The connection between this rigid body and the lower shell element was defined as a tie connection, and the contact between the lower part of the steel tubular part and the concrete was defined as a surface-to-surface contact.

When two surfaces between the lower shell element and

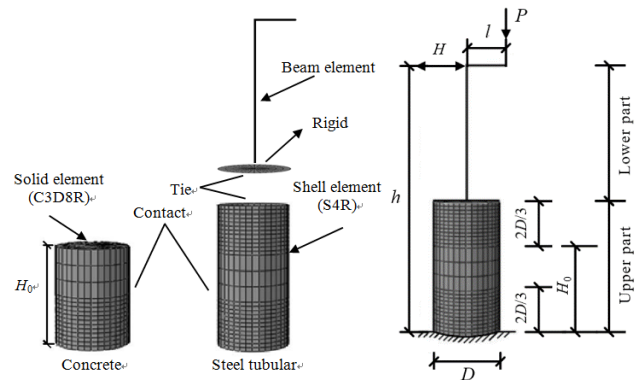


Fig. 2 The finite element model

solid element come into contact, a contact pressure acts on the respective surfaces. This contact pressure was herein calculated by using the hard contact model. When the two surfaces come into contact with each other, frictional stress occurs in the direction tangential to the contact surface. This friction behaviour was expressed by the Coulomb friction model. The resultant shear stress $\tau_{\Sigma} = (\tau_1^2 + \tau_2^2)^{1/2}$ was calculated from the two orthogonal components of the shear stresses τ_1 and τ_2 . The contact surfaces can carry the resultant shear stress τ_{Σ} up to the critical shear stress τ_{cr} before they start to slip. The critical shear stress τ_{cr} is proportional to the contact pressure f and is expressed as

$$\tau_{cr} = \mu f \quad (1)$$

Where μ is the friction coefficient (here, $\mu = 0.4$). If $\tau_{\Sigma} < \tau_{cr}$, no slip displacement occurs between the contact surfaces. If $\tau_{\Sigma} \geq \tau_{cr}$, slip should occur.

To study the effect of the vertical eccentric loading on the seismic performance of a steel tubular bridge pier with partial concrete filling, these 16 models with their different eccentricities were established, and the geometrical dimensions and parameters of the models are summarised in Table 1.

In Table 1, R_t represents radius-thickness ratio of the tube cross-section; λ denotes the slenderness ratio; e represents the eccentricity and $e = lh$; D is the diameter of the tube cross-section; t indicates the thickness of the tube, and R_t and λ can be calculated as follows

$$R_t = \sqrt{3(1-\nu^2)} \frac{\sigma_y}{E} \frac{D}{2t} \quad (2)$$

$$\lambda = \frac{2h}{r} \frac{1}{\pi} \sqrt{\frac{\sigma_y}{E}} \quad (3)$$

Where ν = Poisson's ratio, E = Young's modulus for steel, r = radius of gyration of the cross-section, σ_y = the yield stress of the steel.

$R_t = 0.07, 0.08, \text{ and } 0.09$ and $\lambda = 0.2, 0.3, \text{ and } 0.4$, in accordance with the Japanese seismic design code (Japan Road Association 2016), were chosen to investigate the effect on seismic performance of radius-thickness ratio and slenderness ratio, respectively.

Table 1 Geometrical dimensions and parameters used in the FEM models

| Model | R_t | λ | h (mm) | e | D (mm) | t (mm) | H_0 (mm) |
|-------|-------|-----------|----------|------|----------|----------|------------|
| 1 | 0.07 | 0.2 | 5340 | 0.00 | 2000 | 39 | 1709 |
| 2 | 0.07 | 0.2 | 5340 | 0.10 | 2000 | 39 | 1709 |
| 3 | 0.07 | 0.2 | 5340 | 0.15 | 2000 | 39 | 1709 |
| 4 | 0.07 | 0.2 | 5340 | 0.20 | 2000 | 39 | 1709 |
| 5 | 0.08 | 0.3 | 9140 | 0.00 | 2256 | 39 | 2925 |
| 6 | 0.08 | 0.3 | 9140 | 0.10 | 2256 | 39 | 2925 |
| 7 | 0.08 | 0.3 | 9140 | 0.15 | 2256 | 39 | 2925 |
| 8 | 0.08 | 0.3 | 9140 | 0.20 | 2256 | 39 | 2925 |
| 9 | 0.07 | 0.4 | 10650 | 0.00 | 2000 | 39 | 3408 |
| 10 | 0.07 | 0.4 | 10650 | 0.10 | 2000 | 39 | 3408 |
| 11 | 0.07 | 0.4 | 10650 | 0.15 | 2000 | 39 | 3408 |
| 12 | 0.07 | 0.4 | 10650 | 0.20 | 2000 | 39 | 3408 |
| 13 | 0.09 | 0.2 | 6800 | 0.00 | 2542 | 39 | 2176 |
| 14 | 0.09 | 0.2 | 6800 | 0.10 | 2542 | 39 | 2176 |
| 15 | 0.09 | 0.2 | 6800 | 0.15 | 2542 | 39 | 2176 |
| 16 | 0.09 | 0.2 | 6800 | 0.20 | 2542 | 39 | 2176 |

To ensure that failure occurred at the bottom of each steel tubular pier, the height of in-filled concrete (H_0) was chosen according to provisions of the Japanese seismic design code (Japan Road Association 2016) and a trial-and-error analysis.

The boundary of the FEM models was fixed at the bottom of the column (Fig. 2). These columns were subjected to constant vertical eccentric load P and cyclic horizontal load H at the top of the column. The magnitude of the constant vertical eccentric load P is $0.15P_y$ (P_y is yield axial load of the hollow tube column, which is considered according to existing steel bridge pier dimensions representative of typical circular columns used in Japan (Kinoshita *et al.* 2008). Then the incremented cyclic horizontal load H was applied, which was displacement-controlled as shown in Fig. 3, where δ_0 represents the initial horizontal displacement caused by P as calculated by use of Eq. (4)

$$\delta_0 = \frac{M_0 h^2}{2EI} = \frac{Plh^2}{2EI} \quad (4)$$

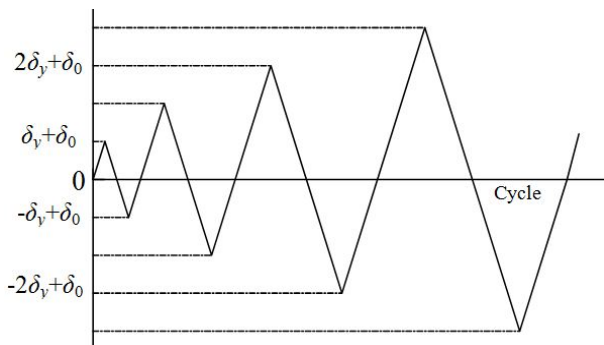


Fig. 3 The horizontal load cycle

Where M_0 = initial moment generated by vertical eccentric loading, where $M = Pl$. Here, δ_y represents the yield horizontal displacement of a non-eccentrically loaded column, as calculated by use of Eqs. (5)-(6)

$$\delta_y = \frac{H_y h^3}{3EI} \quad (5)$$

$$H_y = \frac{2I \cdot \sigma_y}{Dh} \left(1 - \frac{P}{P_y} \right) \quad (6)$$

Where, I is the second moment of area, about the neutral axis, of the hollow steel tube column.

In this numerical analysis, the yield stress of the steel is 345 MPa, the Young's modulus is 206 GPa, and the Poisson's ratio is 0.3. A bilinear stress-strain relationship was used to simulate the steel, and the hardening ratio is assumed to have been 1%. The compressive, and tensile, strengths of the concrete are 22.4 MPa and 2.21 MPa, respectively. The concrete damage plasticity criterion was adopted.

2.2 The validity of the finite element analyses

To verify the validity of the numerical analysis, the testing of four eccentrically loaded steel tube columns with partial concrete filling (tests P1, P2, P3, and P4) was carried out. The materials and structural properties, and the comparison between experimental and analytical results, are summarised in Table 2.

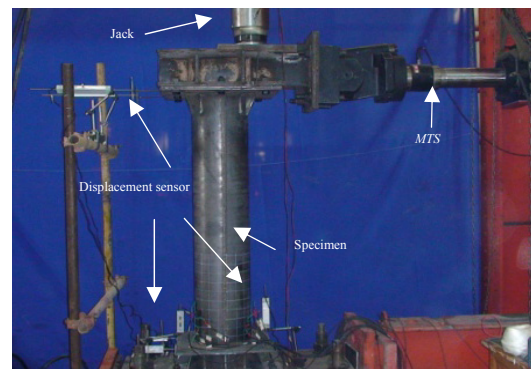
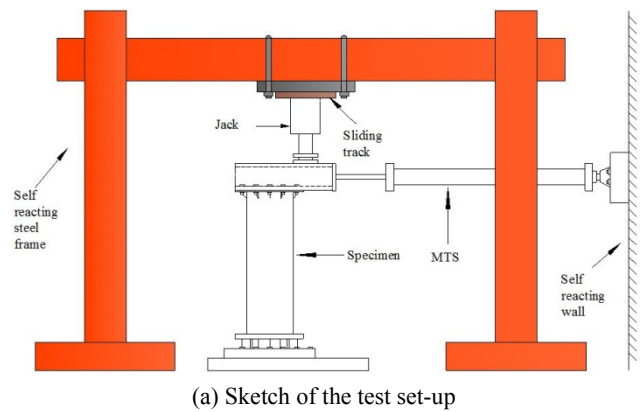


Fig. 4 Test setup

Table 2 Material, structural properties and the comparison between experimental and analytical results

| Specimens | D (mm) | t (mm) | H_0 (mm) | P (kN) | L (mm) | Experimental results | | | Analytical results | | Anal./Exp. | |
|-----------|-------------|-------------|---------------|-------------|-------------|----------------------|------------------|------------------|--------------------|-----------------|------------|----------------------|
| | | | | | | H_u' (kN) | δ_u' (mm) | δ_0' (mm) | H_u (kN) | δ_u (mm) | H_u/H_u' | δ_u/δ_u' |
| P1 | 360 | 5.75 | 615 | 320 | 153 | 183.3 | 46.9 | 1.5 | 168.7 | 37.9 | 0.92 | 0.82 |
| | | | | | | -206.1 | -38.2 | | -197.2 | -30.9 | 0.96 | 0.81 |
| P2 | 360 | 5.75 | 660 | 322 | 306 | 173.3 | 47.9 | 2.1 | 157.6 | 37.3 | 0.91 | 0.80 |
| | | | | | | -245.4 | -34.1 | | -229.9 | -30.6 | 0.93 | 0.90 |
| P3 | 300 | 5.75 | 595 | 281 | 153 | 131.2 | 57.2 | 1.1 | 117.0 | 45.1 | 0.90 | 0.80 |
| | | | | | | -157.3 | -43.7 | | -148.8 | -36.6 | 0.95 | 0.83 |
| P4 | 300 | 5.75 | 618 | 274 | 306 | 110.0 | 52.2 | 1.7 | 98.9 | 44.9 | 0.90 | 0.86 |
| | | | | | | -172.0 | -35.0 | | -160.5 | -30.7 | 0.93 | 0.87 |

*Note: Steel: $\sigma_y = 345$ (MPa); $E = 204$ (GPa); $\nu = 0.28$, $h = 1530$ mm

Concrete: $f_{ck} = 32.4$ (N/mm²); $E_c = 3.45 \times 10^4$ (N/mm²); $\nu = 0.2$

H_u' is the experimental maximum horizontal force; δ_u' denotes the experimental horizontal displacement corresponding to H_u' ; δ_0' is the experimental initial horizontal displacement under vertical eccentric loading P ; H_u is the analytical maximum horizontal force; δ_u represents the analytical horizontal displacement corresponding to H_u .

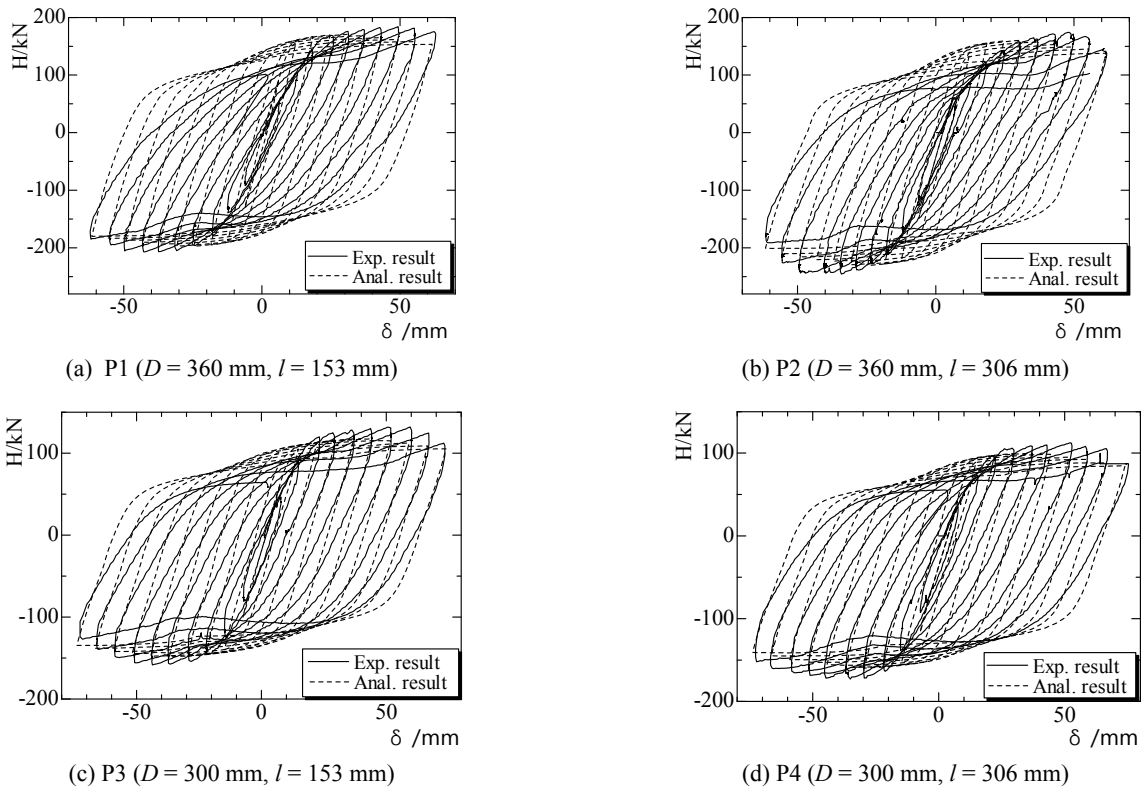


Fig. 5 Comparison of analytical, and experimental, results

Fig. 4 shows the loading device used in these tests. Fig. 4(a) illustrates a sketch of the test set-up; Fig. 4(b) shows the in situ test set-up. The constant vertical loading was applied by way of a jack, and an upper sliding track was installed to ensure that the jack slides freely in the horizontal direction. The horizontal hysteretic displacement was applied by *MTS*. The vertical load was delivered to the foundation by the self-reacting steel frame; the horizontal cyclic load was delivered to the self-reacting wall. The lower end stiffened plate of a test specimen was bolted to

the column base, which was anchored to the laboratory strong-floor. The horizontal load and displacement were measured by *MTS* and displacement transducers, respectively (Fig. 4(b)).

In the experiment, the constant vertical load P was first applied at the top of the test specimen, and then the incremental cyclic horizontal displacement δ was applied as shown in Fig. 3.

Fig. 5 shows the analytical and experimental horizontal load-displacement hysteretic curve of the steel tubular

columns with partial concrete filling. In Fig. 5, the horizontal axis shows the horizontal displacement, the vertical axis indicates the horizontal force, the solid lines show analytical results, and the dashed lines are experimental results (“+” is the *MTS* pull direction, “-” is the *MTS* push direction).

Based on strain gauge measurements, the yielding of steel tubes in specimen P1 occurs at +11.2 mm (or -7.5 mm),

the specimen reaches a maximum reaction force of +183.3 kN (or -206.1 kN). Local buckling occurs at the column base after a displacement of +30.8 mm. In specimen P2, the yielding of the steel tube occurs at +14.6 mm (or -7.6 mm), local buckling occurs at the column base after a displacement of +28.6 mm, and the specimen reaches a maximum reaction force of +173.3 kN (or -245.4 kN). The yielding of the steel in specimen P3 occurs at +12.9 mm (or

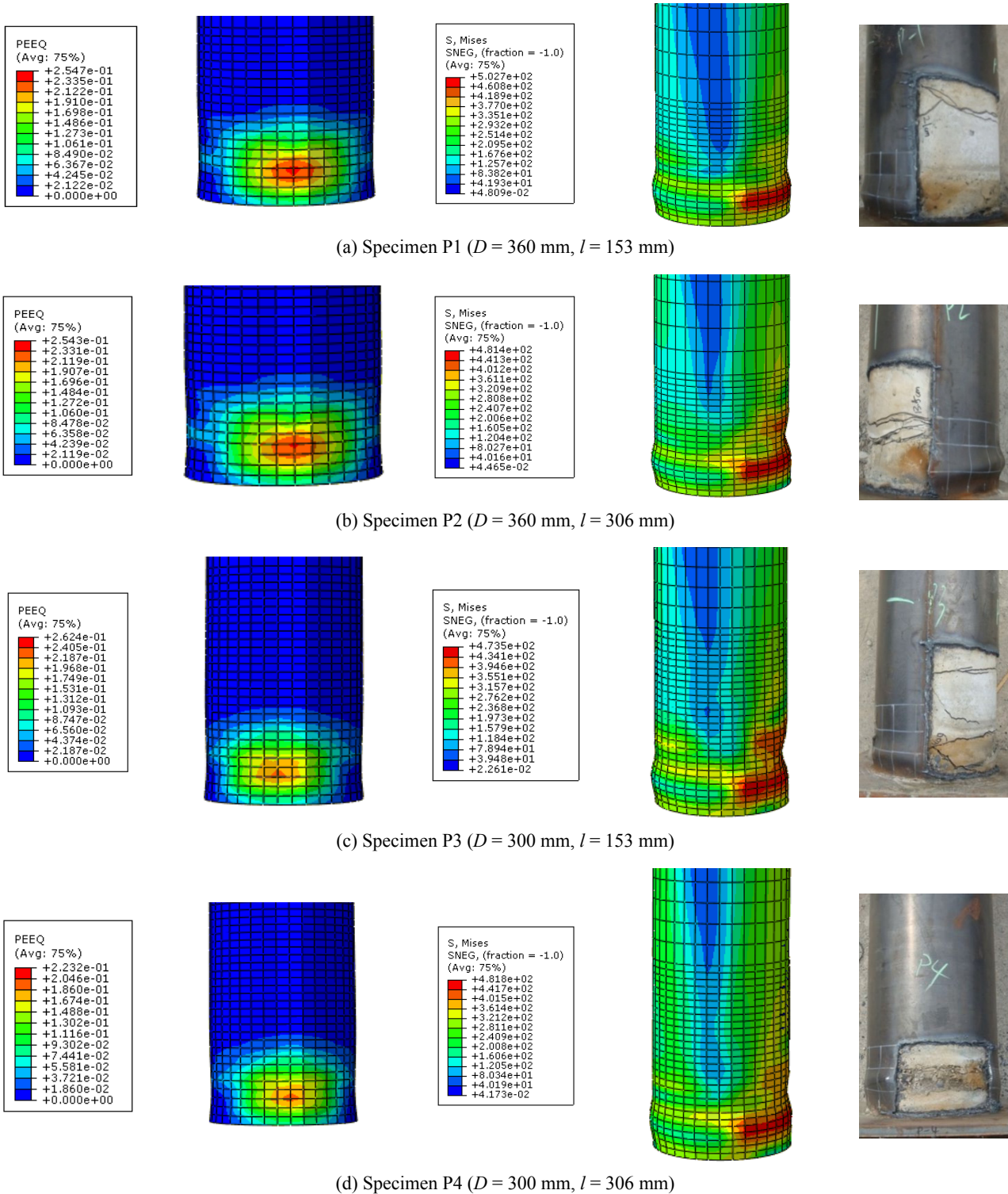


Fig. 6 Final failure states of the four FEM models compared with their experimental counterparts

-9.2 mm), and the maximum reaction force reaches +131.1 kN (or -157.3 kN). In specimen P4, yielding of the steel tubes occurs at +11.8 mm (or -10.8 mm), the maximum reaction force reaches +110 kN (or -172.0 kN). No cracking, or fracturing, of these four specimens was observed.

Based on Fig. 5, it could be found that the finite element analysis accurately simulated the mechanical behavior of the steel tubular columns with partial concrete in-fill; but, in the unloading process, the stiffness predicted by the finite element analysis is greater than that measured experimentally. There are two reasons for this: (1) the in-filled concrete, in those specimens under cyclic loading, is crushed resulting in the reduction of the local stable capacity of the steel tube, which leads to the rapid decline in stiffness in these experiments. In the finite element analysis,

however, the concrete is not rendered ineffective, even if it reaches its ultimate limit state, it exerts no influence on the local stable capacity of the steel tube; (2) in these analyses, the steel material properties are simplified to the form of a bi-linear stress-strain relationship resulting in excessive residual deformation. Based on the data in Table 2, the maximum deviation of the maximum horizontal force and the corresponding deformation are 5% and 20%, respectively.

The failure modes of these experimental specimens, and the corresponding FEA results, are given in Fig. 6. The local buckling position in the FEA model output is consistent with that observed experimentally, and the high-stress distribution region of the concrete coincides with the locus of the damage observed experimentally.

From the aforementioned discussion, the results of the

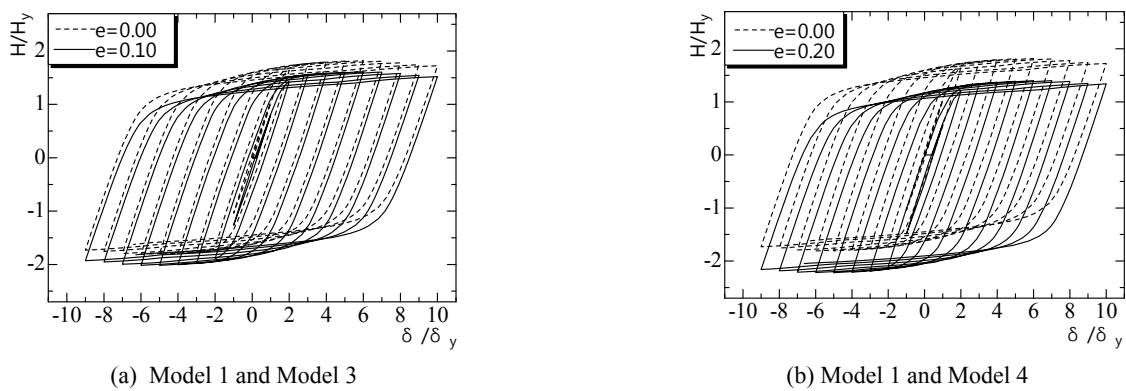


Fig. 7 Comparison of the hysteresis curves of centrally, and eccentrically, loaded models: $R_t = 0.07$, $\lambda = 0.2$

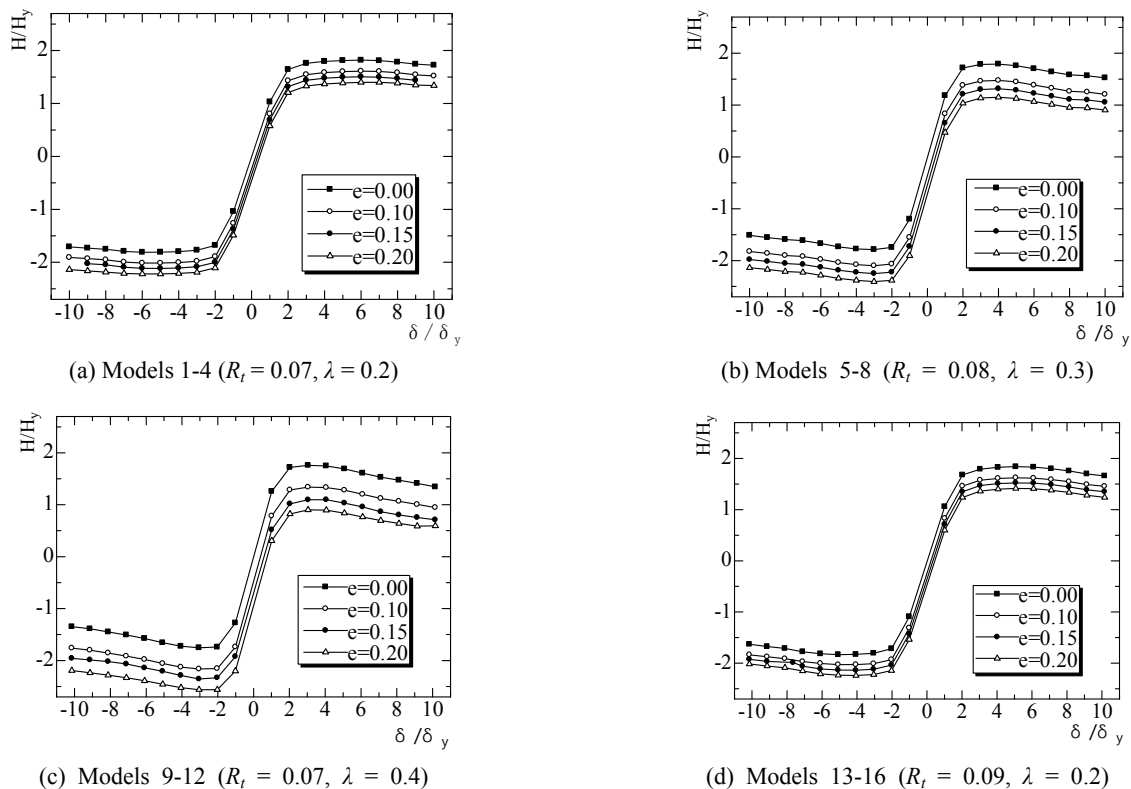


Fig. 8 FEM output data

numerical analysis agree with the experimental results. The validity and the effectiveness of the numerical analysis were thus demonstrated.

3. Finite element analysis results

3.1 The effect of eccentricity on the seismic behavior and the stress distribution

To investigate the effect of eccentricity on the seismic behaviour of the steel tube columns with partial concrete filling, the analytical hysteretic curves of the non-eccentrically, and eccentrically, loaded models with parameters $R_t = 0.07$, and $\lambda = 0.2$ are compared (Fig. 7).

It is observed that the maximum horizontal bearing capacity of the non-eccentric model in the positive direction is almost the same as that in the negative direction, however, the maximum horizontal bearing capacity of the eccentric model in the positive direction is lower than that of the non-eccentric model, and it is improved in the negative direction. The asymmetry is more obvious as the eccentricity increases.

The skeleton curves of all models are shown in Fig. 8. It can be found that the bearing capacity of the eccentric side (the “+” direction) decreases with increasing eccentricity and the capacity on the opposite side (the “-” direction) improves with increasing eccentricity. The more the eccentricity increases, the more obvious this trend becomes: because of the increase in initial moment with the increasing

eccentricity, the seismic performance decreases.

Fig. 9 shows the comparison of the stress distribution and the local buckling of these models for $R_t = 0.08$ and $\lambda = 0.3$ at a displacement level of $\delta/\delta_y = 10$. It can be observed that the locations of the stress distribution zones are similar among these four models. The difference is that the maximum stress on the eccentrically loaded column is lower than that of the non-eccentrically loaded column. The buckling modes of the eccentrically loaded models are almost the same as those of the non-eccentrically loaded models.

3.2 Theoretical analysis of the non-eccentric and eccentric columns

Fig. 10 shows the simplified loading regimes for non-eccentric, and eccentric, columns. H_c and H_e represent the horizontal load on the non-eccentric and eccentric columns. δ_c and δ_e represent the corresponding horizontal displacements, respectively. The values of δ_c and δ_e can be calculated by using Eqs. (7)-(8)

$$\delta_c = \frac{H_c h^3}{3EI} \tag{7}$$

$$\delta_e = \delta_0 + \frac{H_e h^3}{3EI} \tag{8}$$

Therefore, based on Eqs. (4), (7), and (8), the relationship between δ_c and δ_e can be described as in Eq. (9)

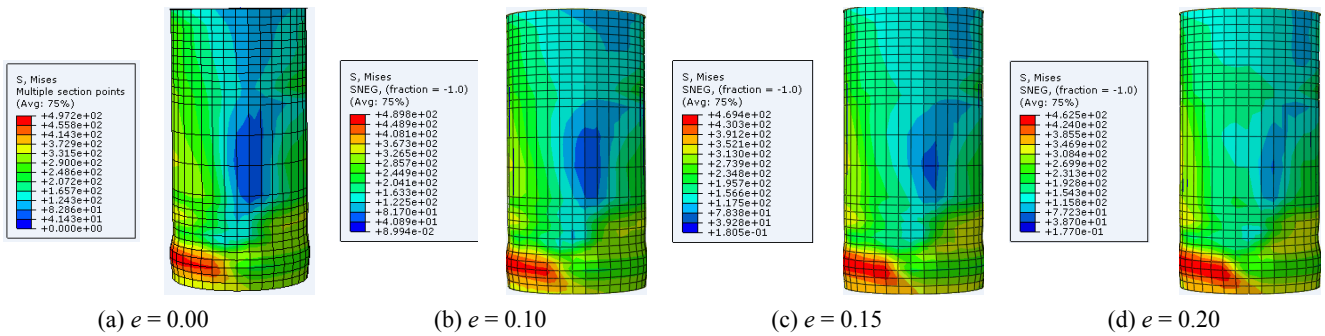


Fig. 9 Comparison of the stress distribution and buckling modes of Models 5-8 ($R_t = 0.08$, $\lambda = 0.3$)

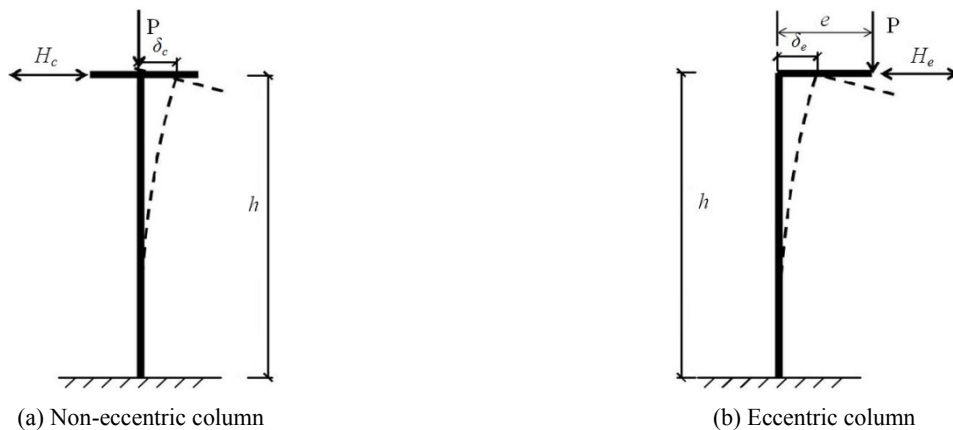


Fig. 10 The structural configurations: non-eccentric and eccentric columns

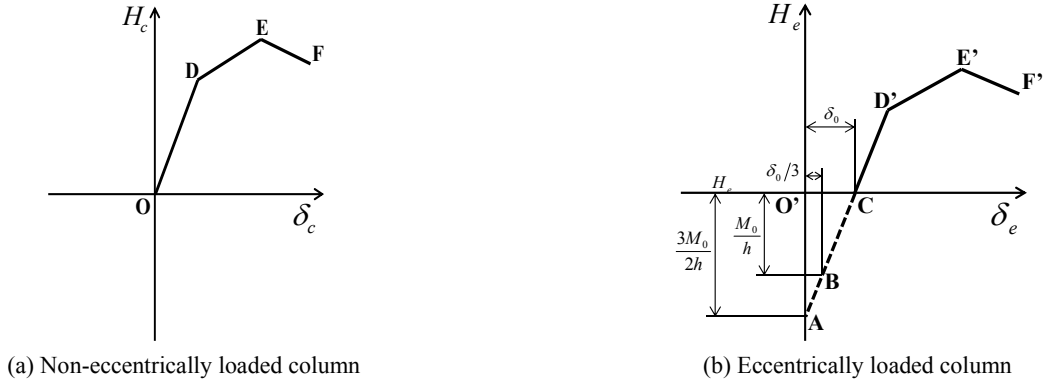


Fig. 11 Sketches of the skeleton curves in the elastic range

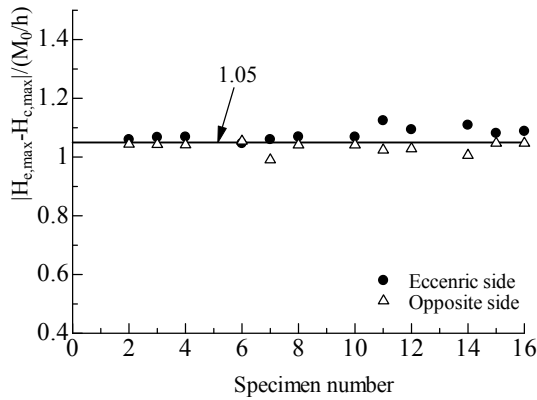


Fig. 12 Comparison of the maximum strength difference across all FEM models

$$\delta_e - \delta_c - \delta_0 = \frac{h^3}{3EI} (H_e - H_c) \quad (9)$$

Where, $\delta_e - \delta_c$ denotes the difference in horizontal displacements between the non-eccentric, and eccentric, columns.

To illustrate the behaviour produced by Eq. (9), three conditions with different $\delta_e - \delta_c$ are discussed: 0, $\delta_0/3$, and δ_0 . Based on Eq. (4), the difference in the horizontal load of the centrally, and eccentrically, loaded columns, $H_e - H_c$, can be expressed by Eqs. 10(a)-(c)

$$H_e - H_c = -3M_0/(2h) \quad \text{for} \quad (\delta_e - \delta_c = 0) \quad (10a)$$

$$H_e - H_c = -M_0/h \quad \text{for} \quad \delta_e - \delta_c = \delta_0/3 \quad (10b)$$

$$H_e - H_c = 0 \quad \text{for} \quad \delta_e - \delta_c = \delta_0 \quad (10c)$$

Fig. 11 is used to explain the relationships given in Eq. (10). Point D (or D') denotes the yield strength state, point E (or E') refers to the maximum strength state and point F (or F') denotes the limit strength state. Fig. 11(a) represents the simplified skeleton curve of the non-eccentric pier column, and Fig. 11(b) demonstrates the skeleton curve of the eccentric pier column.

The first relationship in Eq. (10) illustrates that, in the case of identical displacements, in the elastic range, the

difference in the horizontal force between H_e and H_c is $-3M_0/(2h)$. This result that a point corresponding to Point O in Fig. 11(a) is equivalent to Point A on the ordinate of Fig. 11(b).

The second formula (Eq. 10(b)) indicates that, in the elastic range, when the horizontal displacement $\delta_e - \delta_c = \delta_0/3$, the difference in the horizontal force between H_e and H_c is $-M_0/h$. In this case, the origin O in Fig. 11(a) corresponds to Point B in Fig. 11(b).

Under the same principle, Eq. (10c) implies that a point corresponding to Point O in Fig. 11(a) is Point C in Fig. 11(b).

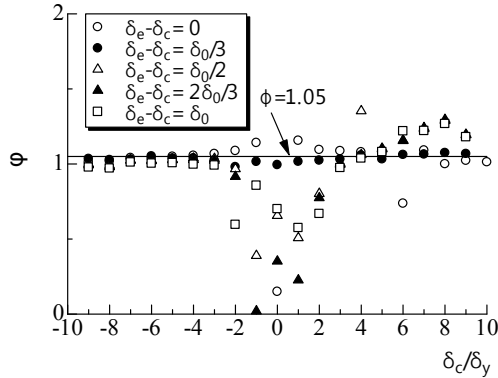
The three cases discussed above show that, with the change in the difference $\delta_e - \delta_c$, the relationship between H_e and H_c varies. It should be noted that all of the above derivation is based on elastic theory; however, large plastic deformations may be induced by severe earthquake events. Therefore, it is necessary to find a relationship between H_e and H_c that is valid in both the elastic, and plastic, ranges. For this purpose, the results obtained from an elasto-plastic large displacement FEA are used.

Fig. 12 shows the statistical results of the maximum strengths of the specimens under non-eccentric, and eccentric, loads. The horizontal axis represents the specimen number, and the vertical axis indicates the difference of the absolute value between the maximum positive and negative strength $[H_{c,max} - H_{e,max}]/(M_0/h)$. $H_{c,max}$ and $H_{e,max}$ represent the maximum bearing capacity of the non-eccentrically, and eccentrically, loaded columns, respectively. According to Fig. 12, the difference between $H_{c,max}$ and $H_{e,max}$ fluctuates around an approximate value of $1.05M_0/h$, and the discrepancies therein are small, so $H_{e,max} - H_{c,max}$ can be given by the following formula

$$H_{e,max} - H_{c,max} = -1.05M_0/h \quad (11)$$

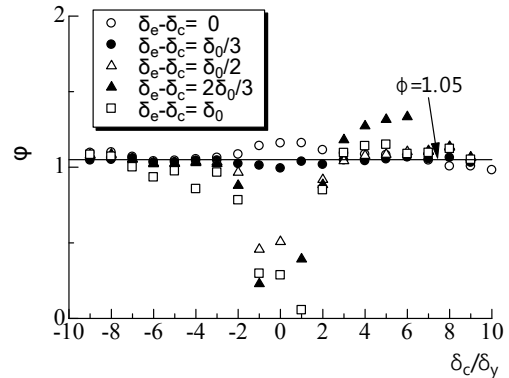
To prove that the Eq. (11) can be applied in an arbitrary loading state, the strength differences at arbitrary displacement levels in two typical models (Models 2 and 4) were compared (Fig. 13). The horizontal axis is δ_e/δ_c , the vertical axis is $[H_c - H_e]/M_0/h$ (designated as parameter φ in the following description), here, H_c and H_e are the horizontal loads at displacements δ_c and δ_e , respectively. In this work, five different values of $\delta_e - \delta_c$ are considered: 0,

$\delta_0/3, \delta_0/2, 2\delta_0/3,$ and δ_0 . The corresponding horizontal load



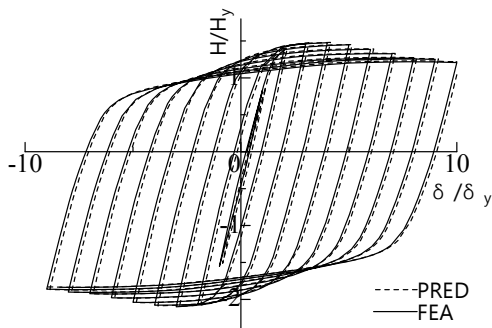
(a) Specimen 2

fluctuates around 1.05.

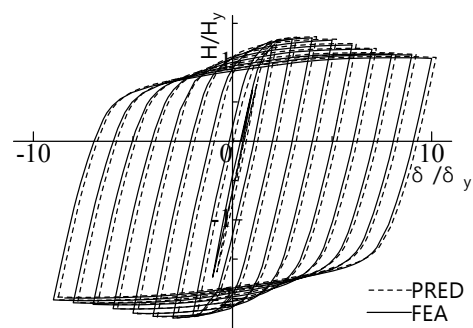


(b) Specimen 4

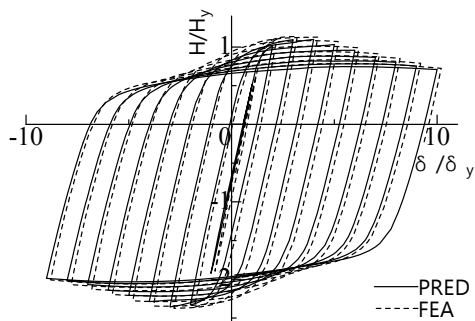
Fig. 13 The horizontal bearing capacity difference comparison for different displacement differences



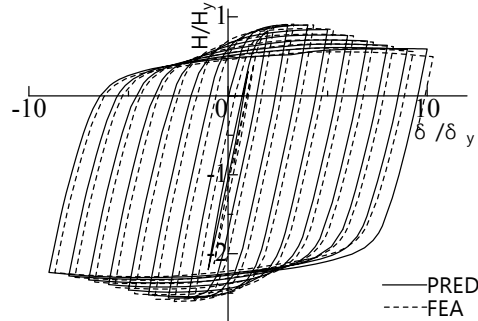
(a) Specimen 6



(b) Specimen 7



(c) Specimen 11



(d) Specimen 12

Fig. 14 The prediction of horizontal force-displacement hysteresis curves for an eccentrically loaded column

in each case is obtained from the finite element analysis.

$$\varphi = [H_c - H_e] / (M_0 / h) \quad (12)$$

From Fig. 13, it can be found that:

- (1) In the elastic range, the difference of the value, φ , becomes quite noticeable. In the case of $\delta_e - \delta_c = 0$ and $\delta_e - \delta_c = 2\delta_0/3$, the values of φ are, respectively, about 1.2 and zero. Among these cases, the value of φ in the $\delta_e - \delta_c = \delta_0/3$ case approaches unity.
- (2) In the plastic range, the value of φ does not vary significantly with changes in $\delta_e - \delta_c$.
- (3) Over the entire range, in the case of $\delta_e - \delta_c = \delta_0/3$, φ

In these five cases, the horizontal strength relationship in the non-eccentric, and eccentric, columns at $\delta_e - \delta_c = \delta_0/3$ case, whether in the elastic and inelastic stages of the structures, matched that given by formula (13)

$$H_e - H_c = -1.05M_0/h \quad (13)$$

3.3 Verification of the validity of the horizontal bearing capacity relationship

Fig. 14 shows the hysteresis curves for some of the partial models. The solid line shows the finite-element analytical results (marked FEM), and the dashed line represents the predicted hysteretic curve of the eccentricity

loaded model (marked PRED), which can be obtained from the analytical results of the simulation of a non-eccentrically loaded column (Eq. (14)).

The calculation process is as follows: (1) the hysteretic curve of the non-eccentrically loaded column is given, namely, the δ_c and $H_c(\delta_c)$ values are known; (2) for an arbitrary value of δ_e , the corresponding horizontal force $H_e(\delta_e)$ can be obtained using the following formula

$$H_e - H_c = -1.05M_0/h \quad (14)$$

From Fig. 14, it can be observed that the predicted hysteresis curves show good agreement with the finite element analytical results in both the elastic, and plastic, ranges. This verified the validity of the aforementioned empirical formula.

4. Conclusions

- (1) With increasing eccentricity, the bearing capacity on the eccentric side of a steel tubular bridge pier with concrete filling is greatly reduced, while the capacity on the opposite side increases. The behavior evinces an obvious asymmetry, and the seismic performance decreases.
- (2) An empirical formula governing the bearing capacity relationship between a non-eccentrically loaded bridge pier, and an eccentrically loaded bridge pier was proposed, and the validity of the empirical formula was verified. This will provide a theoretical basis for the future seismic design of such eccentrically loaded piers.

Acknowledgments

This study is supported by the Project of Education Department of Liaoning Province (serial number: LJQ2014060) and Discipline Content Education Project of Shenyang Jianzhu University (XKHY2-88) and Postdoctoral Science Foundation of Shenyang Jianzhu University (SJZUBSH201607): this support is gratefully acknowledged.

References

- Aoki, T., Suzuki, S., Watanabe, S., Suzuki, M., Usami, T. and Ge, H. (2003), "Experimental study on strength and deformation capacity of inverted L-shaped steel bridge piers subjected to out-of-plane cyclic loading", *Struct. Eng. Earthq. Eng., JSCE*, **724**(62), 213-223. [In Japanese]
- Gao, S.B., Usami, T. and Ge, H.B. (2000a), "Eccentrically loaded steel columns under cyclic in-plane loading", *J. Struct. Eng., ASCE*, **126**(8), 964-973.
- Gao, S.B., Usami, T. and Ge, H.B. (2000b), "Eccentrically loaded steel columns under cyclic out-of-plane loading", *J. Struct. Eng., ASCE*, **126**(8), 974-981.
- Ge, H., Watanabe, S., Usami, T. and Aoki, T. (2003), "Analytical study on strength and deformation capacity of inverted L-shaped steel bridge piers subjected to out-of-plane cyclic loading", *Struct. Eng. Earthq. Eng., JSCE*, **738**(64), 207-218. [In Japanese]
- Goto, Y., Kumar, G. and Kawanishi, N. (2010), "Nonlinear Finite Element Analysis for Hysteretic Behavior of Thin-Walled Circular Steel Columns with In-Filled Concrete", *J. Struct. Eng., ASCE*, **136**(11), 1413-1422.
- Goto, Y., Mizuno, K. and Prosenjit Kumar, G. (2012), "Nonlinear Finite Element Analysis for Cyclic Behavior of Thin-Walled Stiffened Rectangular Steel Columns with In-Filled Concrete", *J. Struct. Eng., ASCE*, **138**(5), 571-584.
- Goto, Y., Ebisawa, T. and Lu, X. (2014), "Local Buckling Restraining Behavior of Thin-Walled Circular CFT Columns under Seismic Loads", *J. Struct. Eng., ASCE*, **140**(5), 1-14.
- Iura, M., Orino, A. and Ishizawa, T. (2002), "Elasto-plastic behavior of concrete-filled steel tubular columns", *Struct. Eng. Earthq. Eng., JSCE*, **696**(58), 285-298. [In Japanese]
- Japan Road Association (2016), Specifications for Highway Designs Part V Seismic Design (English Version), Maruzen, Tokyo, Japan.
- Kim, D., Jeon, C. and Shim, C. (2016), "Cyclic and static behaviors of CFT modular bridge pier with enhanced bracings", *Steel Compos. Struct., Int. J.*, **20**(6), 1221-1236.
- Kinoshita, K., Miki, C. and Ichikawa, A. (2008), "Study on seismic performance of existing steel bridge frame piers with circular column", *Struct. Eng. Earthq. Eng., JSCE*, **64**(3), 571-587. [In Japanese]
- Mamaghani, I.H., Khavanin, M., Erdogan, E. and Falken, L. (2008), "Elasto-plastic analysis and ductility evaluation of steel tubular columns subjected to cyclic loading", *Proceedings of Structures Congress*, Vancouver, Canada, April.
- Michel, B. and Julia, M. (2004), "Seismic design of concrete-filled circular steel bridge piers", *J. Bridge Eng., ASCE*, **9**(1), 24-34.
- Moon, J., Roeder, C.W., Lehman, D.E. and Lee, H.E. (2012), "Analytical modelling of bending of circular concrete-filled steel tubes", *Eng. Struct.*, **42**, 349-361.
- Nie, J.G., Wang, Y.H. and Fan, J.S. (2012), "Experimental study on seismic behavior of concrete filled steel tube columns under pure torsion and compression-torsion cyclic load", *J. Constr. Steel Res.*, **79**, 115-126.
- Perea, T., Leon, R.T., Hajjar, J.F. and Denavit, M.D. (2014), "Full-scale tests of slender concrete-filled tubes: Interaction behavior", *J. Struct. Eng., ASCE*, **140**(9), 1249-1262.
- Sakimoto, T., Nakayama, M., Kawabata, T., Watanabe, H. and Eyama, E. (2002), "Hysteretic behavior of inverted-shaped steel bridge piers subjected to out-of-plane cyclic loading", *Struct. Eng. Earthq. Eng., JSCE*, **696**(54), 215-224. [In Japanese]
- Shimaguchi, Y. and Suzuki, M. (2015), "Seismic performance evaluation of circular steel bridge piers which have damage and concrete filled repair", *Proceedings of LABSE Conference Nara 2015*, Nara, Japan, May.
- Susantha, K.A.S., Ge, H.B. and Usami, T. (2002), "Cyclic analysis and capacity prediction of concrete-filled steel box columns", *Earthq. Eng. Struct. Dyn.*, **31**(2), 195-216.
- Wang, Z.F. and Yamao, T. (2011), "Ultimate strength and Ductility of Stiffened Steel Tubular Bridge Piers", *Int. J. Steel Struct.*, **11**(1), 81-90.
- Wang, Z.F., Wu, Q. and Sui, W.N. (2011), "Effect of Filled-concrete Height on Ultimate Strength and Ductility of Steel Tubular Bridge Pier with Partial Filled-concrete", *Adv. Mater. Res.*, **368**.
- Wang, Z.F., Sui, W.N., Li, G.C., Wu, Q. and Ge, L. (2015), "Mechanical Behavior of Partially Concrete-filled Steel Circular Bridge Piers Under Cyclic Lateral Load", *China J. Highway Transport*, **28**(1), 62-70. [In Chinese]
- Wang, Z.F., Zhang, X. and Li, G.C. (2016), "A simple method to calculate the concrete-filled height of steel tubular bridge piers with concrete-filled based on the ductility performance", *J.*

Shenyang Jianzhu Univ. (Natural Science), **32**(5), 827-837.

[In Chinese]

Wei, H., Wang, H.J. and Hasegawa, A. (2014), "Experimental study on reinforced concrete filled circular steel tubular columns", *Steel Compos. Struct., Int. J.*, **17**(4), 517-533.

CC